Modelling, Simulation, and Performance Analysis of Waterflooding in Naturally Fractured Reservoir

Haruna Yusuf [1], Mohammed Bello Adamu [1], Ibrahim Ayuba [1], Salisu Salihu Alhassan [1], Abdulwahab Giwa [2], Tajuddeen Othman [1]

[1] *Abubakar Tafawa Balewa University*
Tafawa Balewa Way, P. M. B. 0248, Bauchi, 740272, Nigeria

[2] *Federal University Dutsin-Ma*
P. M. B. 5001 Dutsin-ma, Katsina State, Nigeria

DOI: 10.22178/pos.125-6

LCC Subject Category: T1-995

Received 25.11.2025
Accepted 28.12.2025
Published online 31.12.2025

Corresponding Author:
Haruna Yusuf

Abstract. The petroleum industry widely uses water flooding as a secondary recovery technique in petroleum reservoirs; however, in Naturally Fractured Reservoirs (NFRs), dual-porosity and dual-permeability features lead to rapid water breakthrough, poor sweep efficiency, and reduced oil recovery, thereby diminishing the effectiveness of water flooding. Despite the use of packages such as MRST (Matlab Reservoir Simulation Toolbox) and BOAST-NFR (Black Oil Applied Simulation Tool for Naturally Fractured Reservoirs) for analysing water flooding performance in NFR, accurate modelling of matrix–fracture interactions and prediction of breakthrough behaviour remain significant challenges. This study aims to construct a synthetic 3D geological NFR model using MATLAB-MRST and to evaluate water-flooding performance using BOAST-NFR, focusing on reservoir pressure and cumulative production volumes. While limited to synthetic data with a single injector–producer setup, the research is significant for advancing understanding of water flooding in complex fractured systems, offering a cost-effective means of testing scenarios and contributing to improved strategies for NFR management. The water flooding simulation in an NFR using BOAST-NFR revealed typical reservoir-depletion and pressure-drop behaviours. The study concludes that BOAST-NFR is a valuable screening tool for assessing water flooding in dual-porosity reservoirs despite its limitations in modelling matrix-fracture interactions. The result shows cumulative oil production of 1.48 MMSTB (28% recovery factor) after 10 years. It is recommended to maintain output while oil rates are high, apply pressure maintenance and water management strategies, prioritise early production, monitor watercut closely, and evaluate enhanced recovery techniques to maximise ultimate recovery and reservoir longevity.

Keywords: Water flooding; Dual-porosity; Dual-permeability; MATLAB-MRST; BOAST-NFR.

INTRODUCTION

The classifications of primary, secondary, and tertiary (enhanced) oil recovery correspond to distinct phases and techniques of hydrocarbon extraction based on reservoir drive mechanisms and the recovery methods applied [1–3]. Primary recovery relies on natural reservoir energy to produce oil; secondary recovery increases pressure and displaces oil through injection, with waterflooding being the most widely used secondary method [4, 5]. According to authors [6–8], natural Fractured Reservoirs (NFRs) are characterised as complex geological formations comprising fractures and other structural anomalies that significantly influence fluid flow dynamics and hydrocarbon recovery efficiency [9]. These fractures serve as high-conductivity pathways for reservoir fluids, thereby substantially enhancing the reservoir system's overall effective permea-

bility [10]. Furthermore, matrix heterogeneity within NFRs has been identified as a critical factor influencing the development of diverse reservoir strategies [11–13]. NFRs constitute a significant global hydrocarbon resource, accounting for approximately half of the world's total reserves [6, 9, 14, 15].

Fractures are ubiquitous subsurface features [5, 16].

Modelling and simulating Natural Fractured Reservoirs (NFRs) are essential activities for comprehending reservoir behaviour and optimising hydrocarbon recovery performance [17–19]

Common approaches to simulation include unstructured, structured, and discrete-fracture grids. These methods have limitations, including limited flexibility and difficulty updating models with new data [20]. Early contributions, such as the work by Warren and Root cited in [19], introduced analytical solutions for single-phase, unsteady-state flow and pioneered the concept of dual porosity to represent flow between matrix blocks and fractures. Accurate modelling of NFRs requires careful consideration of several important factors, including matrix and fracture porosity and permeability, as well as the transmissibility between the matrix and fracture systems [10].

Naturally fractured reservoirs (NFRs) are complex hydrocarbon deposits that require integrating multiple data sources and fields of study for a comprehensive understanding, as no single method or dataset can fully characterise the reservoir [8]. Naturally fractured reservoirs present significant challenges for reservoir engineering and simulation due to their unique flow dynamics governed by complex fracture networks [21–23]. A review of the literature highlights that the main challenges in developing NFRs arise from the significant permeability contrast between the matrix rock and the fracture network. These challenges include complex reservoir characterisation, difficulty in flow modelling, early breakthrough, low recovery rates, matrix-fracture interactions, and issues with sound design and stimulation.

As identified by the authors [8, 24], experts often categorise the challenges of simulating fluid flow in NFRs into three key areas: adequately modelling the dominant fluid pathways; precise knowledge of permeability within the fracture network; and the need for the model to capture key flow properties accurately.

Various waterflooding strategies are employed to recover hydrocarbons that remain after primary recovery methods, once their economic limits have been reached. In Naturally Fractured Reservoirs (NFRs), fluid injection processes (using water or gas) pose a significant challenge: the injected fluid can readily bypass the low-permeability matrix by preferentially flowing through high-permeability fractures toward production wells [4, 9, 10, 25, 26].

Sophisticated simulation tools such as MRST are essential for accurately modelling the complex geological features of Naturally Fractured Reservoirs (NFRs). Specialised simulators, such as BOAST-NFR, provide the most reliable predictions of current and future NFR performance.

BOAST-NFR simulates dual porosity but lacks independent geological modelling capabilities. This limitation is overcome by integrating it with tools such as MRST, which enables the construction of realistic reservoir geometries and the testing of various flooding scenarios.

This study developed a 3-D synthetic model of an NFR using MRST and simulated its waterflooding performance using BOAST-NFR. The aim is to analyse key production indicators (Np, Gp, Wp) before and after flooding to assess recovery efficiency. This work is significant for improving the understanding of matrix-fracture interactions and offers a cost-effective framework for optimising water-injection strategies in NFRs, thereby aiding field development planning.

METHODS

A naturally fractured reservoir was modelled as a single-layer formation using a 15×1×1 parallel Cartesian grid, with dimensions shown in Table 1. The reservoir is composed of a matrix system with φm = 29% and kx = ky = kz = 1 md. Assumptions for the model include: a fracture network consisting of a single set of parallel fractures with φf = 1%, a diagonal permeability tensor with kf = 90 md, and a fracture spacing of L = 5 ft. A commercial reservoir simulator (MRST) is used to develop a 3-D synthetic model of an NFR. In contrast, a Black oil simulator (BOAST-NFR) is used to simulate the developed model with the model's data. The water flood scheme was simulated according to the steps illustrated in Figure 1.

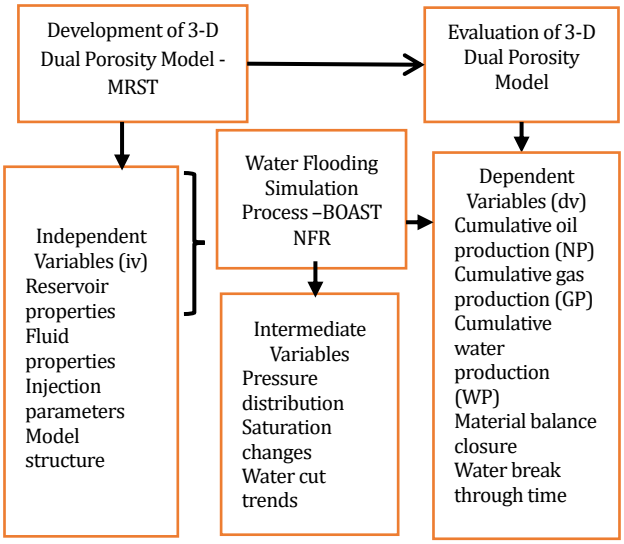

Figure 1 – Flow diagram of the methodology used in this study

Materials and Data. The input data used for this work, presented in Table 1, were obtained from the sixth SPE comparative project on dual-porosity simulators (i.e., NFRs). Some of the fluid-rock properties given in Table 2 and the fluid PVT data presented in Tables 3 and 4 for the project were initially reported by the authors [19, 27] for unfractured reservoirs.

Table 1 – Gridblock and Reservoir Rock Basic Data

Number of gridblocks in the x-direction, nx	15
Number of gridblocks in the y-direction, ny	1
Number of gridblocks in the z-direction, nz	1
Grid size in the x-direction, Δx, ft	400
Grid size in the x-direction, Δy, ft	400
Grid size in the x-direction, Δz, ft	50
Matrix porosity, ϕm, fraction	0.29
Matrix permeability, km, md	1.0
Matrix compressibility, cm, psi-1	$3.5x10^{-6}$
Fracture porosity, ϕf, fraction	0.01
Fracture permeability, kf, md	90
Fracture compressibility, cf, psi-1	$3.5x10^{-6}$
Connate water saturation in the matrix, swc, %	20
Initial pressure, pi, psig	6000
Fracture spacing, L, ft	5

Adopted from authors [19]

Table 2 – Fluid- Rock Properties Data in the Matrix System

Sα	krw	kro	Pcow (psi)
0	0	0	1
0.1	0	0	1
0,2	0	0	1
0.25	0	0.005	0.5
0.3	0.042	0.01	0.3
0.35	0.1	0.02	0.15
0.4	0.154	0.03	0
Sα	krw	kro	Pcow (psi)
0.45	0.22	0,045	-0.2
0.5	0.304	0.06	-1.2
0.6	0.492	0.11	-4
0.7	0.723	0.18	-10
0.75	0.86	0.23	-40
0.8	1	0.23	-40
1	1	0.23	-40

Adopted from authors [19]

The PVT data of oil is divided into two sets. One set corresponds to undersaturated properties relative to a bubble-point pressure, pb = 5545 psig, as presented in Table 3.

Table 2: Undersaturated Oil Properties

Oil density, ρ_o, lb/ft^3	51.14
Oil viscosity at p_b, μ_o, cp	0.21
Slope of μ_o above p_b, $d\mu_o/dp$, cp/psi	$1.72x10^{-5}$
Oil formation volume factor at p_b, B_o, RB/STB	1.8540
Slope of B_o above p_b, dB_o/dp, RB/STB/psi	$-4.0x10^{-5}$

Adopted from authors [19]

Saturated values are shown in Table 4. In this simulation, pressures remain above the bubble-point pressure, and, therefore, mainly undersaturated values are used. PVT data of water are basically μw = 0.35 cp, Bw = 1.07 RB/STB, cw = 3.5×10-6 psi-1 and ρw = 65 lbm/ft3.

Table 4 – Saturated Oil Properties

P (Psi)	μo (cp	Bo (RB/STB)	Rso (SCF/STB)
1674	0.529	1.3001	367
2031	0.487	1.3359	447
2530	0.36	1.3891	564
2991	0.397	1.4425	679
3553	0.351	1.5141	832
4110	0.31	1.5938	1000
4544	0.278	1.663	1143
4935	0.248	1.7315	1285
5255	0.229	1.7953	1413
5545	0.21	1.845	1530
7000	0.109	2.1978	2259

Notes: Adopted from authors [19]

Modelling Using MRST. A synthetic three-dimensional static black oil reservoir model was constructed within the MRST reservoir simulation package, representing a three-dimensional geological structure of a natural fractured reservoir for accurate depiction of geological features like faults, fractures, and variations in rock properties across the reservoir volume, where the fluid properties and rock characteristics are considered fixed (static). It contained one layer in the X, Y, Z grid block, with 15×1×1 cells. The dimensions of the grid blocks are 400ft in the X direction, 400ft in the Y direction, and 50ft in the Z direction. The injection well was placed at (1, 1, 1), while the production well was placed at (15, 1, 1).

Simulation. The simulation of oil production from the synthetically modelled reservoir lasted for 10 years. The researchers imported the data used to develop the MRST model into BOAST-NFR to evaluate water-injection performance in oil recovery. They constrained fluid withdrawal to a total liquid production rate of 800 STB/D, initially controlling water injection at a constant rate of 1,568 STB/D, and limiting bottom-hole pressure to 6,100 psig.

RESULTS AND DISCUSSION

Figure 2 represents a 15x1x1 3-D geological model of a naturally fractured reservoir with matrix in grey colour, fracture in blue colour, and initial oil and water saturations before water flooding. Figure 3a and 3b represent the final oil and water saturations, respectively, after water flooding.

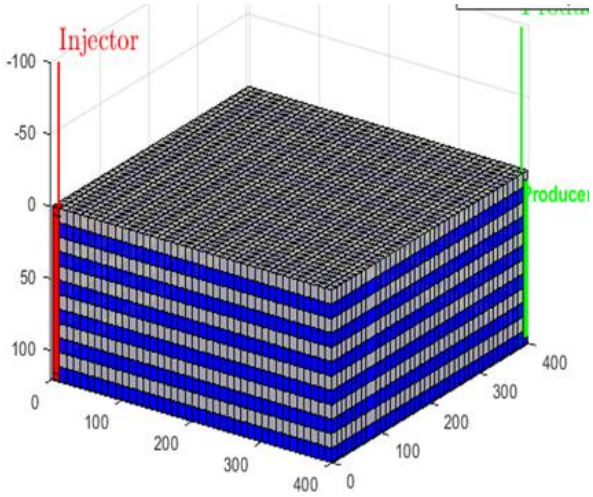

Figure 2 – 3D Geological Model of Natural Fractured Reservoir

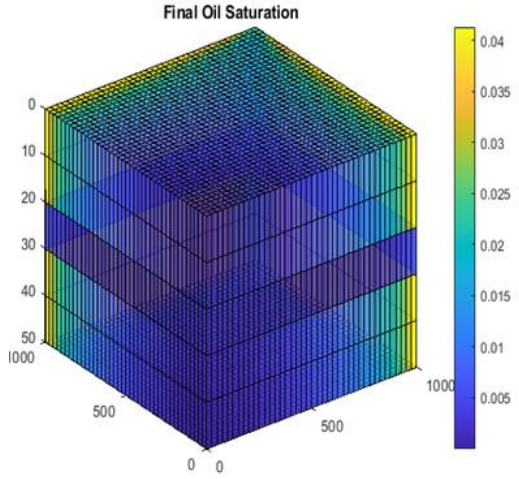

Figure 3a – Final oil Saturation

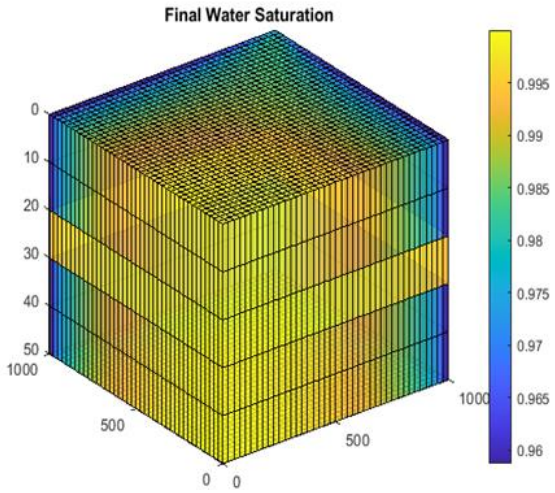

Figure 3b –Final Water Saturation

As shown in Table 5, the average pressure distribution in both the matrix and the fracture is equal, indicating that pressure is evenly distributed in the reservoir and that there is good pressure communication between the matrix and the

fracture. The initial oil saturation is higher in the fracture (0.2, 200%) than in the matrix, but at the end of the simulation, the final oil saturation is higher in the matrix (0.59387, 98%) than in the fracture. Matrix starts at 0.8 (80% of pore volume oil) and gradually declines to 0.60 by 3500 days. The decline is smooth, i.e, oil is being displaced steadily by water injection.

Water saturation: the matrix starts with connate water at 0.20 and gradually increases to 0.40 by the end of the simulation. While the fracture initially was dry, with nearly zero, it then increased sharply to 0.99 by 3467.5 days, confirming that fractures are quickly water-infiltrated and then act as water conduits. The gas saturation indicates that gas in both systems remains negligible; this means there is no significant solution-gas drive; i.e., the system is water-flood-dominated chiefly.

Table 5 – Cumulative production volumes and average reservoir Pressure before and after water injection

Time elapsed	Pres. Dist in mat.	Pres dis. In frac	Oil Sat in the mat.	Oil Sat in farc	Water Sat in the mat.	Water Sat. in frac	Gas Sat. in mat	Gas Sat. I'm frac
0.0001	600.1	600.1	0.8	1	0.2	0.0000006	0	0
182	5934.3	5934.3	0.7862	0.7733	0.2138	0.2267	0	0
365	5927.2	5927.2	0.7667	0.6728	0.2333	0.3271	0	0
547.5	5922.9	5922.9	0.7468	0.5883	0.2532	0.4117	0	0
730	5920.1	5920.1	0.7269	0.5072	0.2731	0.4928	4.00E-09	0
912.5	5919.1	5919.1	0.7075	0.4297	0.5721	0.2925	6.00E-10	8.00E-08
1095	5920.6	5920.6	0.6891	0.3523	0.3109	0.6477	3.00E-07	0
1277.5	5925.3	5925.2	0.672	0.2845	0.328	0.7155	0.00E+00	2.00E-07
1460	5932.09	5932.09	0.65693	0.22641	0.34307	0.77359	0.00E+00	1.80E-07
1642.5	5939.25	5939.25	0.64401	0.1771	0.35599	0.8229	0.00E+00	1.70E-07
1825	5946.88	5946.88	0.63325	0.13655	0.36675	0.86345	0.00E+00	1.60E-07
2007.5	5953.99	5953.99	0.2456	0.10382	0.37544	0.89618	0.00E+00	1.50E-07
2910	5960.4	5960.4	0.61773	0.07737	0.38227	0.922263	0.00E+00	1.50E-07
2372.5	5965.92	5965.92	0.61251	0.0566	0.38749	0.9434	0.00E+00	1.00E-07
2555	5970.41	5970.41	0.60862	0.04072	0.39138	0.95928	0.00E+00	1.50E-07
2737.5	5973.92	5973.92	0.60577	0.02885	0.39423	0.97115	0.00E+00	1.50E-07
2920	5976.55	5976.56	0.60372	0.02018	0.39628	0.9782	0.00E+00	1.60E-07
3102.5	5978.48	5978.48	0.60225	0.01395	0.39775	0.98605	0.00E+00	1.50E-07
3285	5979.86	5979.87	0.60119	0.00956	0.39881	0.99044	2.40E-07	1.40E-07
3467.5	5980.84	5980.84	0.60043	0.00656	0.39957	0.99344	2.20E-07	1.40E-07

Table 6 indicates that the injection performance (Q_{wi}, W_i) is negative, reflecting water injection into the reservoir (input rather than production). The increasing magnitude of cumulative injected water (W_i) indicates a sustained water flooding effort to maintain reservoir pressure. The sweep efficiency ($E_{s\%}$ %) or recovery factor gradually increases from 0% to around 11% during the early simulation time, suggesting modest recovery improvement from water injection. The recovery efficiency (E_s%) increase indicates incremental gains from water flooding, though relatively low due to limited matrix contribution and bypassing effects.

Table 6 – Output results from BOAST

Time	Pave (psi)	Qo (stb/d)	Qg (Mscf/d)	Qw (stb/d)	Np (STB)	Gp (Mscf)	WP (STB)	Qwi	Wi	Es %	GOR
0.0001	6000.1	800.0	1224.0	0.0	0.08	0.1	0.0	-2102.1	-0.21	0.0	1529.96
182	5934.3	799.9	1223.9	0.1	145598.5	222760.2	1.5	-1339.1	-231148	2.8	1529.96
365	5927.2	797.6	1220.2	2.4	291819.2	446472.3	180.8	-1345.2	-47704.8	5.5	1529.96
547.5	5922.9	791.7	1211.2	8.3	436907.1	668451.4	1092.9	-1343.7	-722435	8.3	1529.96
730	5920.1	778.5	1191.1	21.5	580341.1	887899.9	3658.9	-1336.9	-967142.9	11.0	1529.96
912.5	5919.1	751.5	1149.7	48.5	720229.1	1101923.4	9770.9	-132.3	-1209878	13.6	1539.96
1095	5920.6	702.4	1074.6	97.6	853279.3	1305574.0	22720.7	-1292.0	-144588	16.2	1530.00
1277.5	5925.3	629.0	962.4	171.0	975077.7	1492188.0	46922.3	-1244.0	-1680226	18.5	1529.96
1460	5932.1	542.8	830.5	257.2	1082054	1656067.0	85946.5	-1184.9	-1901923	20.5	1529.96
1642.5	5939.3	458.5	701.4	341.5	1173471	1796122.0	140529.2	-1126.4	-2112833	22.2	1529.96
1825	5946.9	374.3	572.6	425.7	1249371	1912415.6	210629.1	-1067.7	-2313003	23.7	1529.96

Time	Pave (psi)	Qo (stb/d)	Qg (Mscf/d)	Qw (stb/d)	Np (STB)	Gp (Mscf)	WP (STB)	Qwi	Wi	Es %	GOR
2007.5	5954.0	298.5	456.7	501.5	1310600	2006258.0	295399.8	-1014.2	-2502861	24.8	1529.96
2910	5960.4	231.3	354.0	568.7	1358800	2080161.0	393199.8	-966.8	-2683526	25.7	1529.96
2372.5	5965.9	174.5	267.0	625.5	1395663	2136718.0	502337.1	-926.4	-2856158	26.4	1529.96
2555	5970.4	128.8	197.1	671.2	1423172	2178965.0	620828.2	-893.7	-3022118	26.9	1529.96
2737.5	5973.9	93.5	143.0	706.5	1443304	2209925.0	746696.3	-868.4	-3182793	27.3	1529.96
2920	5976.6	67.1	102.7	732.9	1457830	2232311.0	878169.9	-849.3	-3339436	27.6	1529.96
3102.5	5978.5	47.9	73.3	752.1	1468223	2248374.0	1013777.0	-835.5	-3493095	27.8	1529.96
3285	5979.9	34.2	52.3	765.8	1475637	2259877.0	1152363.0	-825.5	-3644598	27.9	1529.96
3467.5	5980.8	24.6	37.6	775.4	1480944	2268153.0	1293056.0	-818.5	-3794569	28.0	1529.96

Water–Oil Ratio (WOR) increases over time, confirming increasing water production and potential water channelling through fractures. On the other hand, the Gas–Oil Ratio (GOR) remains constant around 1530 SCF/STB, indicating stable gas–liquid equilibrium under black-oil assumptions.

The initial production phase is dominated by high oil and low water output, indicating effective displacement. As time progresses, fracture-dominated flow leads to early water breakthrough, evidenced by rising Q_w and WOR, which is typical in a dual-porosity system where injected fluids preferentially flow through fractures rather than sweep the matrix efficiently. These results demonstrate the complex interaction between matrix and fracture systems and highlight the need for accurate dual-porosity modelling to optimise injection strategies.

Surface Fluid Production Rates Variation with Time. From the graph above, the behaviour of Q_o (surface oil production rate) in the initial stage, from year 0, started high (800 bbl/d) and remained relatively stable until the second year, when the decline phase began and continued until reaching the tenth year. Q_o shows a consistent, steep decline over time, reaching near zero at the tenth year; this is because the reservoir's surface oil production diminishes, typical of primary depletion, reservoir pressure decline, and water breakthrough. The behaviour of Q_g (surface gas production rate) is similar to that of Q_o. It started at 1223.97MSCF and gradually declined. Over the long term (6 to 10 years), Q_g decreases steadily, approaching zero, indicating that the reservoir is depleted by the end of the simulation. The internal reservoir flow rate initially increases as pressure differentials drive oil toward the wellbore, and then declines as the reservoir depletes or pressure drops. The water production rate Q_w increases progressively from zero at the beginning, indicating no water production initially. Then rises sharply after year three, reaching approximately 780.95 bbl/day by year ten. The implication of increasing water production suggests water breakthrough or water coning, common in mature reservoirs, which reduces oil production efficiency. High water production complicates separation and increases operational costs.

The Key observations and implications are that the peak production and decline indicate that the initial high oil and gas production rates (Q_o) and Q_g reflect effective reservoir management and pressure support. The decrease in Q_o after about two years indicates reservoir depletion or pressure decline. While the Q_w impact increases significantly after year three, it correlates with the decrease in Q_o. High water production (above 700bbl/day) at the end of the period indicates that a large portion of the produced fluids is water, which diminishes net oil recovery. The graph effectively captures reservoir behaviour over its productive life, clarifying the depletion trends of Q_o, Q_g, and Q_w.

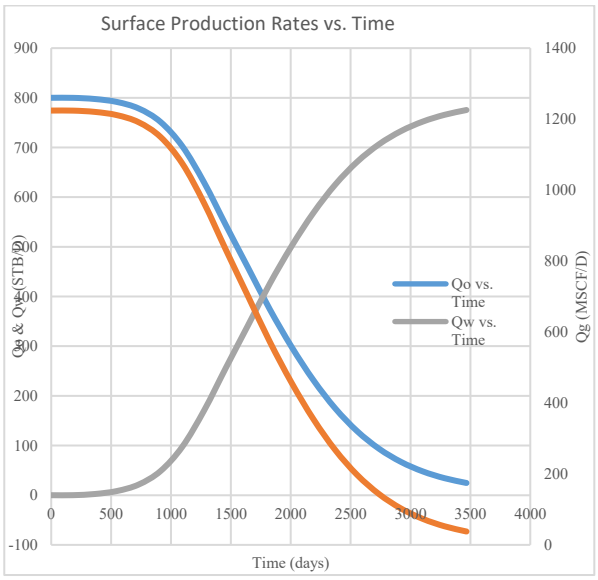

Figure 4 – Surface Oil, Gas and Water Production rates vs time (days)

Pave Variation with Time. From the graph (Figure 5), initially, the reservoir pressure decreases sharply from around 6000 psi to approximately

5912 psi during the first two years, indicating a rapid pressure decline due to fluid production (oil, water, and gas). After reaching this minimum value, the pressure begins to recover gradually, showing a steady upward trend from about the second year onward. By the end of the tenth year period, the pressure approaches its initial value, reaching 5980 psi.

This pattern suggests an initial drawdown phase followed by a pressure buildup or recharge phase, driven by water flooding and support pressure stabilisation processes within the reservoir. The graph shows how reservoir pressure evolves: initially declining sharply, then recovering gradually as the reservoir approaches a new equilibrium. The Pave (average pressure) declines steadily from an initial high of 6000 psi at 0 years to 5,919.11 psi at 2.5 years. Then the pressure increases slowly until it reaches 5981.494 psi at year ten. From two to two and a half years, it indicates the pressure stabilisation point. The parabolic curve during pressure stabilisation is probably due to the matrix-fracture interaction.

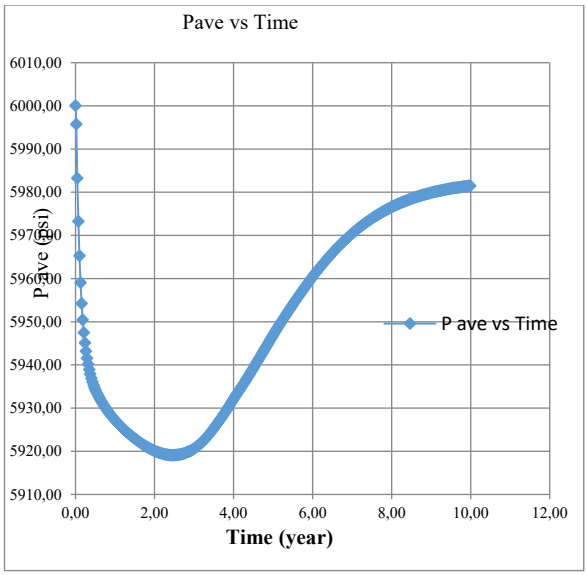

Figure 5 – Pressure Variation with Time

Variation of Surface Cumulative Production Volumes: Np, Gp, Wp, with Time. The Np (Cumulative Oil production) shows a monotonic increase from zero years to around the fifth year, with the rate of accumulation possibly slowing from the fifth to approximately the sixth and a half years as the reservoir depletes. There is an early rapid increase, followed by a gradual levelling off near the end, indicating a decline in oil recovery rates. As for the Gp (Cumulative Gas production) case, it increases over time and follows a similar trend to Np. The rate of increase may vary, reflecting changes in reservoir pressure and solution gas content. The WP (cumulative production) starts low and gradually increases as the reservoir matures. Typically accelerated after initial years, indicating water breakthrough or secondary water drive effects.

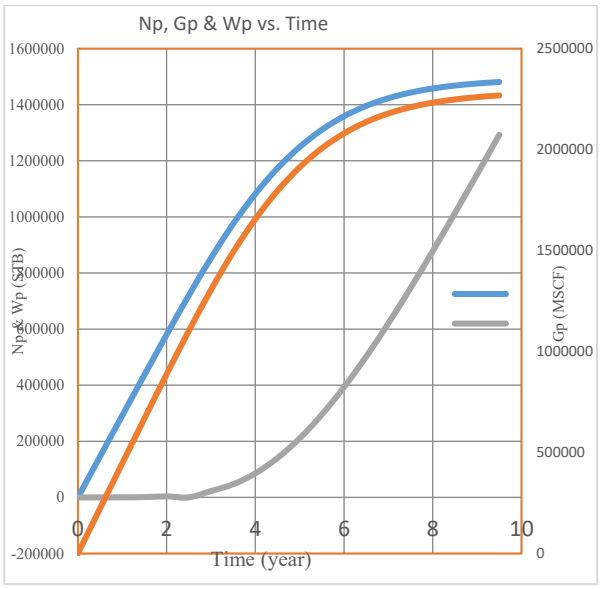

Figure 6 – Cumulative Volumes with Time

CONCLUSIONS

1) The 3-D synthetic geological NFR model was developed using MATLAB-MRST, which accounts for matrix-fracture interactions, fluid saturations, and well positions.

2) Water flooding was simulated in the developed fractured reservoir model using BOAST-NFR, with one injector and one producer vertical wells placed at opposite ends of the reservoir.

3) The water flooding performance was evaluated, resulting in the following:

a) The residual volumes of oil, water, and gas in place are 3.8 MMSTB, 4.6 MMSTB, and 5.8 BSCF, respectively.

b) Cumulative production volumes reached 1.4 MMSTB (28% R.F) for oil, 1.3 MMSTB (60% of initial vol.) of water and 2.3BSCF (28% R.F) after 3650 days of simulation.

c) Researchers observed water breakthrough at 1,460 days.

Overall, the results of this study indicated that though the capability of BOAST-NFR to accurately simulate and predict performance of water

flooding in dual-porosity systems is compounded with uncertainty in: a) Fracture-Matrix Interaction; b) Early Water Breakthrough and c) Poor Sweep Efficiency.

It, however, serves as a rapid, real-time screening tool for dual-porosity reservoirs during candidate selection for water-flooding programs.

REFERENCES

1. Ahmed, T. (2010). *Reservoir Engineering Handbook* (4th ed). Elsevier.
2. Gbadamosi, A., Patil, S., Kamal, M. S., Adewunmi, A. A., Yusuff, A. S., Agi, A., & Oseh, J. (2022). Application of polymers for chemical enhanced oil recovery: A review. *Polymers, 14*(7), 1433. doi: 10.3390/polym14071433
3. Tunio, S. Q., Tunio, A. H., El Adawy, Z. M. & Ghirano, N. A. (2011). Comparison of Different Enhanced Oil Recovery Techniques for Better Oil Productivity. Retrieved from https://www.semanticscholar.org/paper/Comparison-of-Different-Enhanced-Oil-Recovery-for-Tunio-Tunio/862ececbfdf83617c70c3bf547673f76734394bb
4. Karimova, M., Kashiri, R., Pourafshary, P., & Hazlett, R. (2023). A review of wettability alteration by spontaneous imbibition using Low-Salinity water in naturally fractured reservoirs. *Energies, 16*(5), 2373. doi: 10.3390/en16052373
5. Morrow, N., & Buckley, J. (2011). Improved oil recovery by Low-Salinity waterflooding. *Journal of Petroleum Technology, 63*(5). doi: 10.2118/129421-ms
6. Ordonez, A., Penuela, G., Idrobo, E. A., & Medina, C. E. (2001). Recent advances in naturally fractured reservoir modelling. *Ciencia, Tecnología y Futuro, 2*(2).
7. Ayuba, I., Akanji, L. T., & Gomes, J. (2025). Numerical quantification of gas adsorption in unconventional shale rocks. *Fuel, 396*, 135246. doi: 10.1016/j.fuel.2025.135246
8. Bratton, T., Viet Canh, D., Van Que, N., Duk, N. V., Nunt, P. G. D., Li, B., Ray, R. M., Montaron, B., Nelson, R., Schoderbek, D., & Sonneland, L. (2006). The Nature of Naturally Fractured Reservoirs. *Oilfield Review, 18*, 4-23.
9. Hameli, F. A., Suboyin, A., Kobaisi, M. A., Rahman, M. M., & Haroun, M. (2022). Modelling fracture propagation in a Dual-Porosity system: Pseudo-3D-Carter-Dual-Porosity model. *Energies, 15*(18), 6779. doi: 10.3390/en15186779
10. Dean, R. H., & Lo, L. L. (1988). Simulations of naturally fractured reservoirs. *SPE Reservoir Engineering, 3*(02), 638–648. doi: 10.2118/14110-pa
11. Aljuboori, F. A., Lee, J. H., Elraies, K. A., Stephen, K. D., & Memon, M. K. (2022). Modelling the transient effect in naturally fractured reservoirs. *Journal of Petroleum Exploration and Production Technology, 12*(10), 2663–2678. doi: 10.1007/s13202-022-01463-8
12. Moldabayeva, G., Ismailova, J., Khussainova, A., Delikesheva, D., & Ismailov, A. (2025). Waterflood assessment in carbonate reservoirs. *Heliyon, 11*(11), e43386. doi: 10.1016/j.heliyon.2025.e43386
13. Ringrose, P., & Bentley, M. (2014b). The Rock Model. In *Reservoir Model Design*, 13–59. doi: 10.1007/978-94-007-5497-3_2
14. Geiger, S., Dentz, M., & Neuweiler, I. (2011). A novel multi-rate dual-porosity model for improved simulation of fractured and multi-porosity reservoirs. *SPE Reservoir Characterisation and Simulation Conference and Exhibition*. doi: 10.2118/148130-ms
15. Kharrat, R., & Ott, H. (2023). A comprehensive review of fracture characterisation and its impact on oil production in naturally fractured reservoirs. *Energies, 16*(8), 3437. doi: 10.3390/en16083437
16. Hawez, H. K., Sanaee, R., & Faisal, N. H. (2021). A critical review of coupled geomechanics and fluid flow in naturally fractured reservoirs. *Journal of Natural Gas Science and Engineering, 95*, 104150. doi: 10.1016/j.jngse.2021.104150

17. Ayuba, I., Akanji, L. T., Gomes, J. L., & Falade, G. K. (2021). Investigation of Drift Phenomena at the Pore Scale during Flow and Transport in Porous Media. *Mathematics, 9*(19), 2509. doi: 10.3390/math9192509

18. Benali, A., Bacetti, A., Belkherroubi, A., Harhad, H., & Fasla-Louhibi, S. (2017). Fluid flow simulation through a naturally fractured reservoir with MATLAB & Eclipse software. *A- Fundamental and Engineering Sciences, 16*, 19–27.

19. Thomas, L. K., Dixon, T. N., & Pierson, R. G. (1983). Fractured reservoir simulation. *Society of Petroleum Engineers Journal, 23*(01), 42–54. doi: 10.2118/9305-pa

20. Soleimani, M. (2017). Naturally fractured hydrocarbon reservoir simulation by elastic fracture modelling. *Petroleum Science, 14*(2), 286–301. doi: 10.1007/s12182-017-0162-5

21. Azim, R. A. (2022). Finite Element Model to Simulate Two-Phase fluid flow in naturally fractured oil Reservoirs: Part I. *ACS Omega, 7*(31), 27278–27290. doi: 10.1021/acsomega.2c02223

22. Ugwu, A. A., & Moldestad, B. M. (2018). Simulation of Horizontal and Vertical Waterflooding in a Homogeneous Reservoir using ECLIPSE. *Linköping Electronic Conference Proceedings, 142*, 735–741. doi: 10.3384/ecp17142735

23. Li, W., Frash, L. P., Lei, Z., Carey, J. W., Chau, V. T., Rougier, E., Meng, M., Karra, S., Nguyen, H. T., Rahimi-Aghdam, S., Bažant, Z. P., & Viswanathan, H. (2022). Investigating poromechanical causes for hydraulic fracture complexity using a 3D coupled hydro-mechanical model. *Journal of the Mechanics and Physics of Solids, 169*, 105062. doi: 10.1016/j.jmps.2022.105062

24. Debra, A., Ellis, B., Noel, D., & Walmart, A. (2025). Optimising Water Flooding Strategies Using Numerical Simulation for Undersaturated Oil Reservoirs. Retrieved from https://www.researchgate.net/publication/390280756_Optimizing_Water_Flooding_Strategies_Using_Numerical_Simulation_for_Undersaturated_Oil_Reservoirs

25. Madhawee Anuththara, J. G., Moldestad, B. M. E., Kumara, A. S., & Moradi, A. (2023). *Simulation and analysis of waterflooding oil recovery through advanced horizontal wells.* (Thesis; University of South-Eastern Norway).

26. Jonoud, S., Wennberg, O. P., Casini, G., & Larsen, J. A. (2013). Capturing the effect of fracture heterogeneity on multiphase flow during fluid injection. *SPE Reservoir Evaluation & Engineering, 16*(02), 194–208. doi: 10.2118/147834-pa

27. Firoozabadi, A., & Thomas, L. K. (1990). Sixth SPE Comparative Solution Project: Dual-Porosity Simulators. *Journal of Petroleum Technology, 42*(06), 710–763. doi: 10.2118/18741-pa